JOURNAL OF SPACECRAFT AND ROCKETS
Vol. 33, No. 4, July–August 1996

Slosh Dynamics Coupled with Spacecraft Attitude Dynamics Part 2: Orbital Environment Application

R. J. Hung,* Y. T. Long,† and Y. M. Chi‡
University of Alabama in Huntsville, Huntsville, Alabama 35899

Coupling of slosh dynamics within a partially filled rotating Dewar of superfluid helium II with spacecraft attitude dynamics is investigated in response to environmental disturbances including 1) lateral impulses, 2) gravity gradient, and 3) *g*-jitter forces. The purpose of this study is to investigate 1) how a rotating bubble of superfluid helium II reacts to the various environmental disturbances in conjunction with spacecraft attitude dynamics, 2) how amplitudes of slosh reaction forces and torques are induced and are activating on the Dewar coupled with attitude dynamics in response to impulse and environmental disturbances, and 3) how spacecraft translational displacement, velocity, and acceleration deviating from normal spacecraft operation are induced by the slosh dynamics driven by these disturbances. The numerical computation of slosh dynamics is based on a rotational frame, whereas the attitude dynamics is based on a nonrotational frame. The results show that major contributions to attitude dynamics are driven by the coupling with slosh dynamics. Not considering the effect of slosh dynamics acting on the spacecraft may lead to the wrong results for the development of guidance and attitude control techniques.

Introduction

TO carry out scientific experiments, some experimental spacecraft use cryogenic cooling for observation instrumentation and to maintain the temperature near absolute zero for mechanical stability. Most often, the cryogen used is helium II. In this study, coupling of spacecraft attitude dynamics with sloshing dynamics driven by orbit environmental disturbances is investigated. These orbit environmental disturbances include lateral impulses and gravity gradient and *g*-jitter forces. The spacecraft uses the cooling and boiloff from the liquid helium Dewar as a cryogen and propellant to maintain the cooling of instruments, attitude control, and drag-free operation of the spacecraft. Fluid management problems may arise from asymmetric distribution of liquid helium and vapor and also from perturbations in the liquid–vapor interface. Basic understanding of the coupling of slosh dynamics with the six degrees of freedom of the attitude dynamics plays a significant role in the development of spacecraft guidance and attitude control systems.

The mathematical formulation and theory for the coupling of slosh-dynamics fluid motions in a spinning spacecraft Dewar activated by environmental disturbances including 1) lateral impulse,[1] 2) gravity gradient,[2–4] and 3) *g*-jitter[5–7] accelerations with spacecraft attitude dynamics, have been presented in Part 1 of this paper.[8] A computational algorithm for the coupling between helium II slosh dynamics and attitude dynamics has also been discussed and illustrated in Part 1 (Ref. 8).

To study the transient phenomena of coupling between environmental-disturbance-driven slosh reaction forces and torques on the one hand and spacecraft attitude dynamics on the other, we have solved simultaneously for 1) the slosh dynamics in a fluid dynamics formulation and 2) the attitude dynamics in a translational and rotational formulation of spacecraft dynamics. This has been done numerically with the help of the formulation and computational algorithm presented in Part 1 (Ref. 8). Coupling between slosh dynamics and attitude dynamics is shown to affect deeply the behavior of a bubble driven by slosh dynamics, which is quite different from the conclusions obtained earlier[1,9–14] without taking into account the effect of attitude dynamics. Furthermore, attitude dynamics driven by slosh dynamics can cause the spacecraft to deviate from normal operation.[6,10] The results of the present study show that slosh dynamics can 1) create additional time-dependent force, torque, and mass-center fluctuations perturbing the normal spacecraft operational systems, 2) drive progressive variations of the spacecraft Eulerian angles, and 3) cause the spacecraft displacement, velocity, and acceleration to deviate from normal operation.

Received May 15, 1995; revision received March 9, 1996; accepted for publication March 18, 1996.

*Professor, Mechanical and Aerospace Engineering. Associate Fellow AIAA.
†Senior Research Scientist, Department of Mechanical and Aerospace Engineering.
‡Research Assistant, Department of Mechanical and Aerospace Engineering.

Coupling of Helium II Slosh Dynamics and Attitude Dynamics

The characteristics of the three types of orbit environmental disturbances acting on fluid systems are quite different. Lateral impulses are in the form of spotty δ functions with a short time period of 10^{-2} s, whereas both the gravity gradient[10–13] and *g*-jitter[13,14] forces have continuous spectra covering the whole spacecraft orbital period. The magnitudes of these accelerations vary from 10^{-2} to $10^{-9} g_0$ ($g_0 = 9.81$ m/s^2), and they act on fluid elements at different locations with different magnitudes in the case of gravity gradient forces but with same magnitude in the case of impulse and *g*-jitter forces. These differences are summarized in Table 1 of Part 1 (Ref. 8).

Lateral-Impulse-Driven Sloshing

It is assumed that a lateral impulse with the following forms of force $\boldsymbol{F}$ and torque $\boldsymbol{M}$ act on the spacecraft system in the noninertial (rotating) frame with Cartesian coordinates[1–9]:

$$\boldsymbol{F} = (F_x, F_y, F_z) = (20, 0, 0)\ \text{N}$$
$$\boldsymbol{M} = (M_x, M_y, M_z) = (0, 10, 0)\ \text{N}\cdot\text{m} \tag{1}$$

for $0 \le t \le 10^{-2}$ s and

$$\boldsymbol{F} = (0, 0, 0)\ \text{N}$$
$$\boldsymbol{M} = (0, 0, 0)\ \text{N}\cdot\text{m} \tag{2}$$

for $t > 10^{-2}$ s. With a spacecraft mass of 637.6 kg, the lateral impulse is equal to $3.2 \times 10^{-3} g_0$ in this case. In general, the magnitude of lateral impulses ranges from 10^{-2} to $10^{-9} g_0$.

The entire computations of slosh dynamics are carried out in coupling with spacecraft dynamics. The slosh dynamics concluded from the present study are quite different from the results obtained earlier[1,9] without considering the spacecraft dynamics. Figure 1

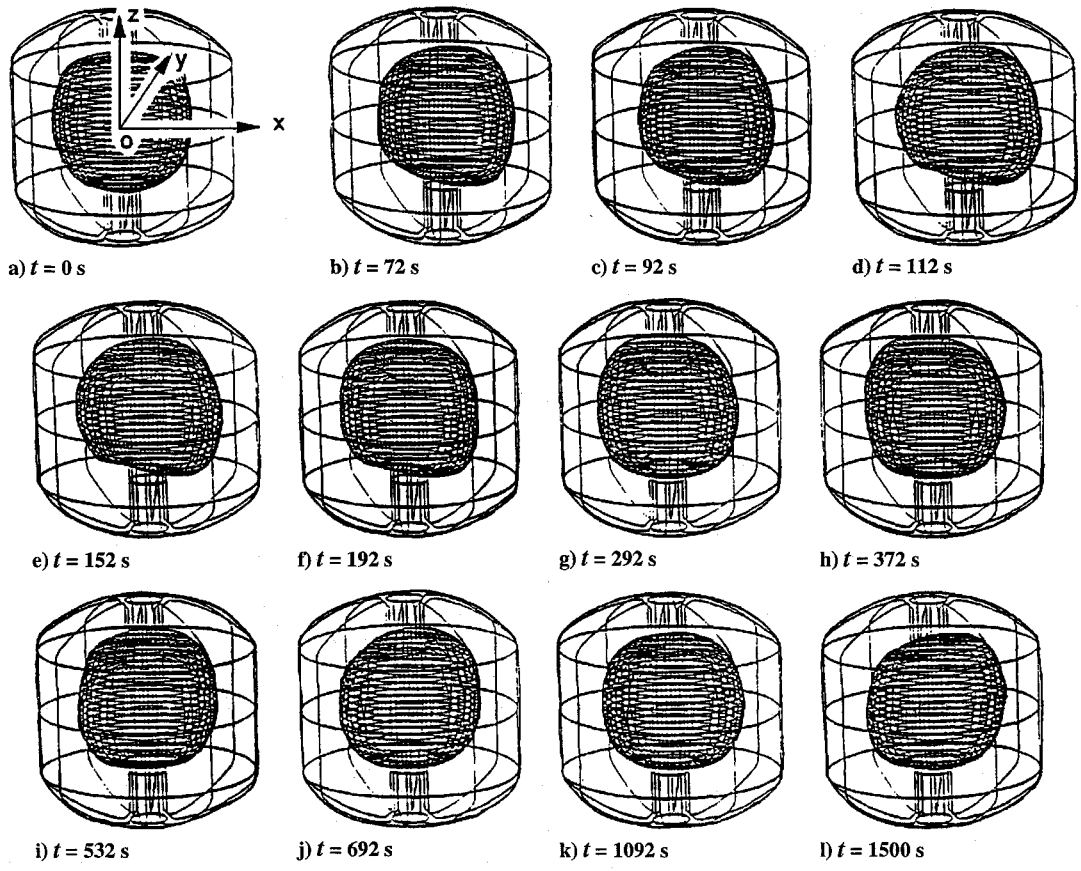

Fig. 1 Three-dimensional bubble deformations in response to lateral impulse.

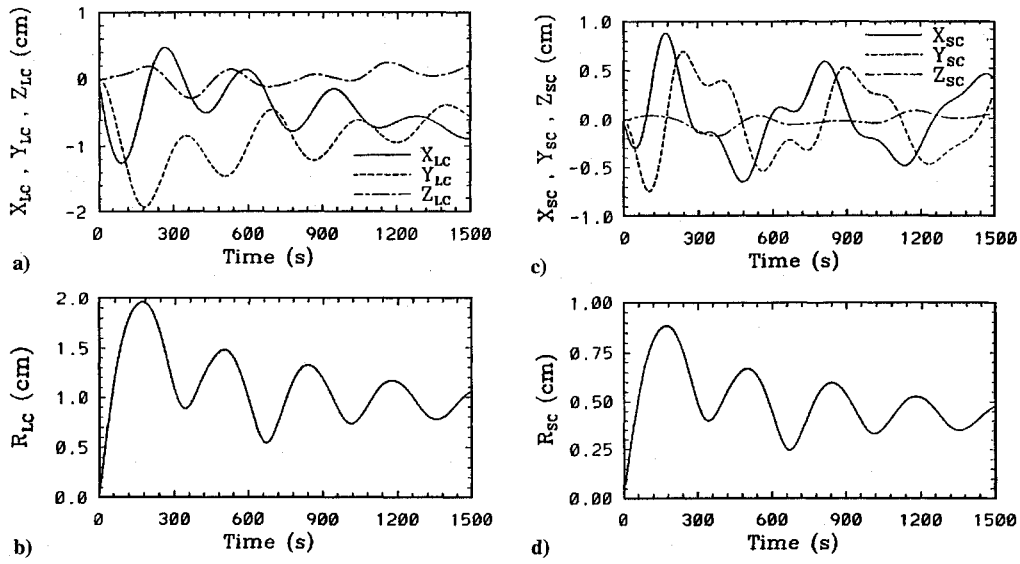

Fig. 2 Time evolution of fluid and spacecraft mass-center fluctuations in response to lateral impulse: a) fluid mass center in (x, y, z) components (rotating frame), b) fluid mass center (absolute value), c) spacecraft mass center in (X, Y, Z) components (nonrotating frame), and d) spacecraft mass center (absolute value).

shows the time evolution of the three-dimensional dynamical behavior of the liquid–vapor interface (bubble) oscillations (in the rotating frame) activated by a lateral impulse acting on the spacecraft in the positive x direction and reacting on the fluid in the negative x direction (thus forcing the bubble in the positive x direction). This time sequence displays the following behavior of the bubble dynamics in response to the lateral impulse: 1) the bubble was first shifted in the positive x direction (the liquid in the negative x direction); 2) the bubble was also shifted in the positive y direction by the Coriolis force due to rotation about the z axis in the rotating frame; and 3) oscillating bubble deformations are seen throughout the 1500-s time span of the simulation.

Figure 2a shows the time evolution of the growth and decay of fluid mass-center fluctuations (in the rotating frame) in response to a lateral impulse. These fluctuations also arise from the torque of the impulse acting about the y axis, which drives slosh-dynamic disturbances propagating along the z axis. The values of the maximum and minimum coordinates of the fluid mass-center

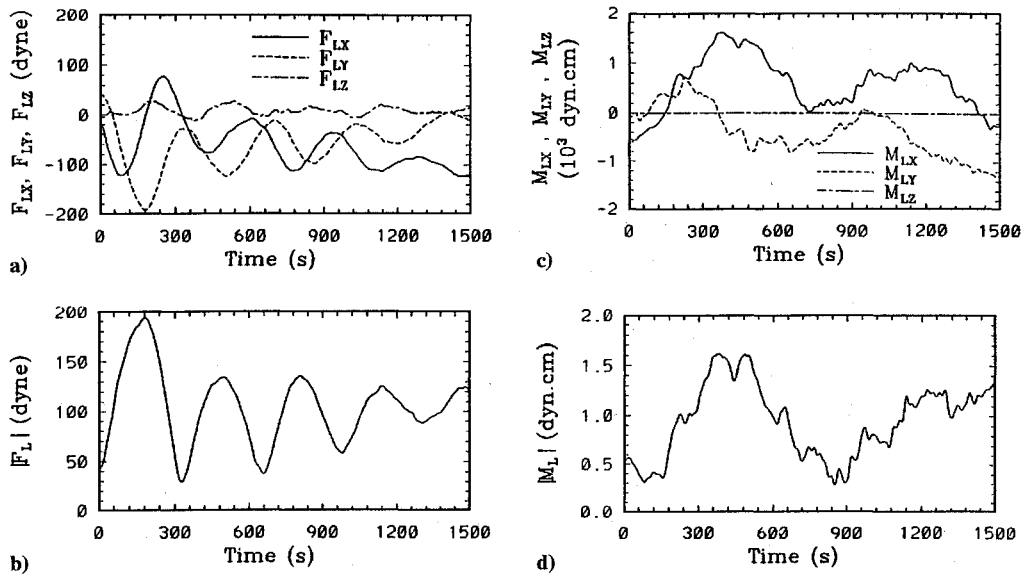

Fig. 3 Time evolution of slosh reaction force and torque (rotating frame) in response to lateral impulse: a) slosh reaction force in (x, y, z) components, b) absolute value of slosh reaction force, c) slosh reaction torque in (x, y, z) components, and d) absolute value of slosh reaction torque.

fluctuations are $\text{Max}(x_{LC}, y_{LC}, z_{LC}) = (0.46, 10^{-4}, 0.25)$ cm and $\text{Min}(x_{LC}, y_{LC}, z_{LC}) = (-1.3, -1.9, -0.28)$ cm, respectively, and the amplitudes of the maximum fluid mass-center fluctuations are $\text{Max}(\Delta x_{LC}, \Delta y_{LC}, \Delta z_{LC}) = (1.73, 1.93, 0.53)$ cm. We see that $\Delta y_{LC} > \Delta x_{LC} > \Delta z_{LC}$.

The response to a lateral impulse can be described as follows:

1) Fluid mass was shifted initially the negative x direction by the Dewar reaction force acting on the fluid in response to the impulse acting on the spacecraft in the positive x direction.

2) Fluid mass-center fluctuations in the negative y direction in the rotating frame were caused by the Dewar reactional Coriolis force acting on the fluid in response to the impulse.

3) The major fluid mass-center fluctuations are in the negative-x and negative-y quadrant of the x–y plane with small ripple oscillations along the z axis.

4) There is a time lag of 150 s between the impulse acting on the spacecraft and the maximum fluid mass-center fluctuation displacement. In other words, the fluid mass center fluctuation grows rather slowly.

5) Figure 2b presents a time history of the fluid mass-center fluctuations, showing an exponential decay with very long time constant because of the extremely low surface tension and viscosity of helium II.

Spacecraft system mass-center fluctuations (in the nonrotating frame) have also been studied and are illustrated in Fig. 2c. The values of the maximum and minimum coordinates in the spacecraft mass-center fluctuations are $\text{Max}(X_{SC}, Y_{SC}, Z_{SC}) = (0.85, 0.63, -0.24)$ cm and $\text{Min}(X_{SC}, Y_{SC}, Z_{SC}) = (-0.6, -0.76, -0.50)$ cm, respectively, and the amplitudes of the maximum spacecraft mass-center disturbances are $\text{Max}(\Delta X_{SC}, \Delta Y_{SC}, \Delta Z_{SC}) = (1.46, 1.39, 0.26)$ cm. We see that $\Delta X_{SC} > \Delta Y_{SC} > \Delta Z_{SC}$ in the nonrotating frame. The spacecraft mass-center fluctuations are very similar to those of the fluid as shown in Figs. 2a and 2b in this subsection, except that the former are shown in the nonrotating frame and the latter in the rotating frame, in which the Coriolis force transfers disturbance from the X to the Y axis. The magnitude is smaller for spacecraft mass-center fluctuations than for fluid mass-center fluctuations by the ratio of the liquid weight to the total spacecraft weight. Figure 2d shows the time history of the spacecraft mass-center displacement. Clearly the effects of helium slosh on the spacecraft attitude control systems must be considered.

In this study, characteristics of the slosh reaction force and torque fluctuations exerted on the Dewar in response to lateral impulses acting on the spacecraft are investigated. The mathematical formulation of the fluctuations of slosh reaction forces and torques exerted on the Dewar has been given earlier.[15,16] With its use, one can calculate the slosh reaction force and the associated torque acting on the Dewar.

Figure 3a shows the computed time variation of the fluctuations of the slosh reaction force (in the rotating frame) exerted on the Dewar in response to the impulse acting on the spacecraft. This figure shows the following results:

1) The values of the slosh reaction force fluctuations are $(\Delta F_{Lx}, \Delta F_{Ly}, \Delta F_{Lz}) = (201, 233, 45.6)$ dynes, so that $\Delta F_{Ly} > \Delta F_{Lx} > \Delta F_{Lz}$. The maximum absolute values of the slosh reaction force are $\text{Max}(|F_{Lx}|, |F_{Ly}|, |F_{Lz}|) = (123, 192, 18.2)$ dynes. Hence $|F_{Ly}| > |F_{Lx}| > |F_{Lz}|$, which coincides with the tendency of the fluid mass-center fluctuations, $\Delta y_{LC} > \Delta x_{LC} > \Delta z_{LC}$.

2) The major slosh reaction forces exerted by the fluid system on the Dewar are in the x–y plane, and there is a small ripple of fluctuations along the z axis induced by the torque of the impulse acting on the spacecraft along the y axis.

3) The slosh reaction force from the fluid system is exerted on the container in response to the impulse with a very small time lag (about 10^{-3} s delay). As a matter of fact, the pattern of F_{Lx} in the first 0.05 s is almost a duplication of that of the lateral impulse acting on the spacecraft with a negative sign, except that the amplitude of the slosh reaction force is smaller than that of the input amplitude because of the damping effect of the fluid system. There are no F_{Ly} and F_{Lz} components of slosh reaction forces during the first 0.05 s. This is quite a contrast to the shifting of the fluid mass center x_{LC}, which reaches its maximum value at time $t = 150$ s, that is, 150 s after the action of the impulse. There is a time delay of the peak values between F_{Ly} and F_{Lx} due to the Coriolis effect of the rotating container shifting from the x to the y axis in the rotating frame. A 100-s phase shift in time for the peak value of F_{Ly} after F_{Lx} is shown in Fig. 3a. This makes the direction of the total resultant forces of slosh-dynamics-modulated fluid reaction forces on the container vary sinusoidally from $\theta = 30$ to 60 deg in the rotating frame. Figure 3b shows the time dependence of the absolute value of the slosh reaction force acting on the Dewar.

4) The damping of the slosh reaction force acting on the Dewar in response to the impulse is shown in both Figs. 3a and 3b. The figures show that the fluids act as a damper of the oscillation arising from the impulse acting on the fluid system.

Figure 3c shows time variations of the slosh reaction torque (in the rotating frame) exerted on the Dewar in response to a lateral impulse acting on the spacecraft. The values of the slosh reaction torque fluctuations are $(\Delta M_{Lx}, \Delta M_{Ly}, \Delta M_{Lz}) = (2.17, 2.03, 10^{-4}) \times 10^3$ dyne · cm, and the maximum absolute values of the slosh reaction torque are $\text{Max}(|M_{Lx}|, |M_{Ly}|, |M_{Lz}|) = (1.56, 1.30, 10^{-4}) \times 10^3$ dyne · cm. This figure shows the following results:

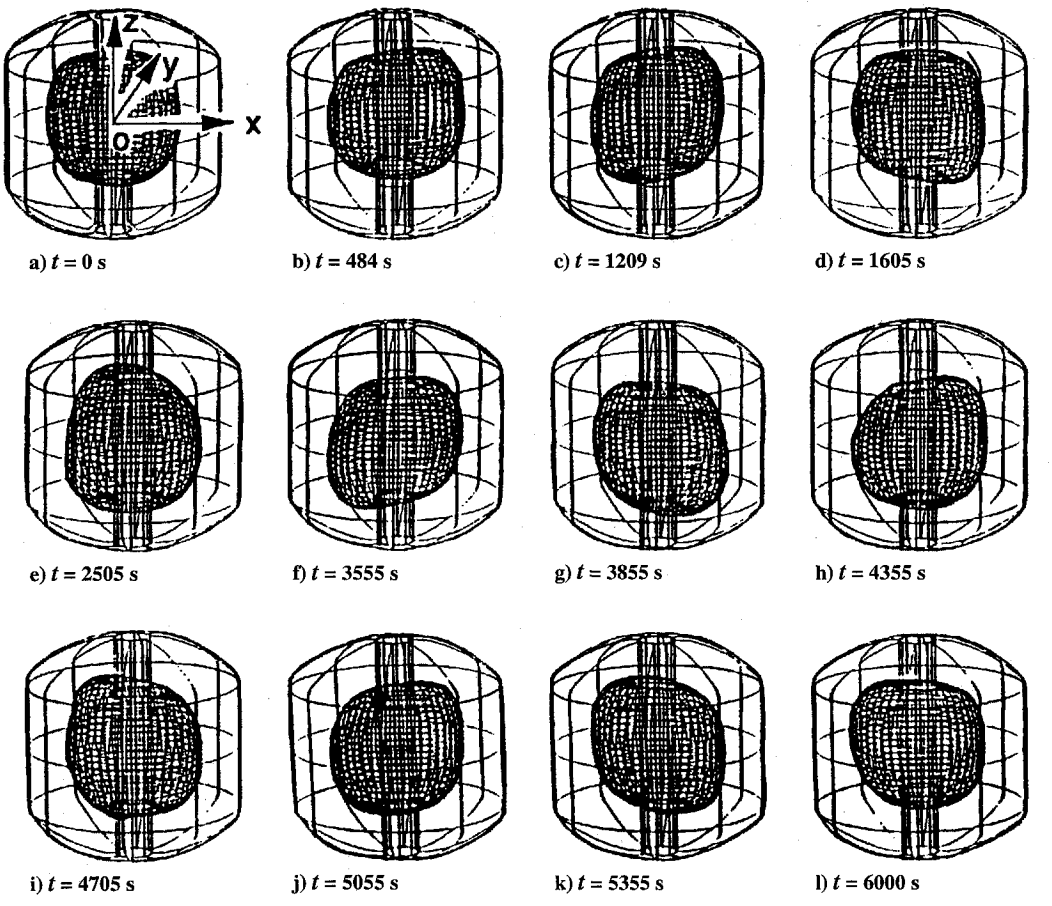

a) $t = 0$ s b) $t = 484$ s c) $t = 1209$ s d) $t = 1605$ s

e) $t = 2505$ s f) $t = 3555$ s g) $t = 3855$ s h) $t = 4355$ s

i) $t = 4705$ s j) $t = 5055$ s k) $t = 5355$ s l) $t = 6000$ s

A) Three-dimensional oscillations

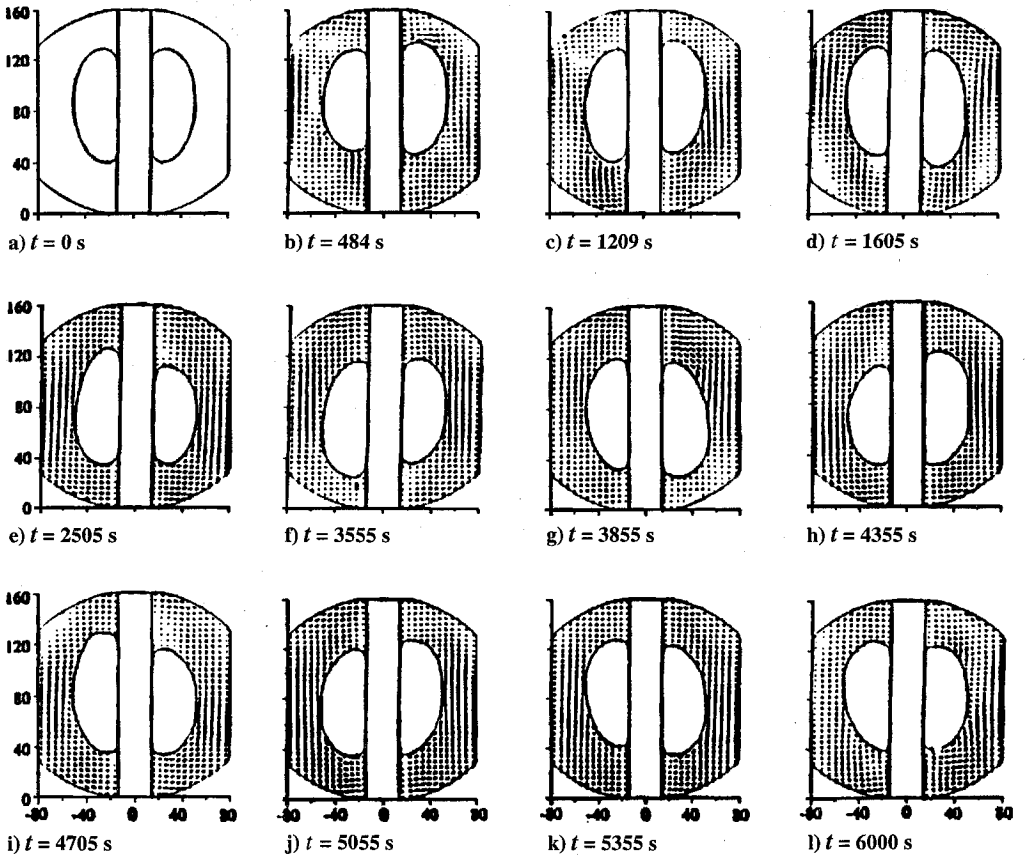

a) $t = 0$ s b) $t = 484$ s c) $t = 1209$ s d) $t = 1605$ s

e) $t = 2505$ s f) $t = 3555$ s g) $t = 3855$ s h) $t = 4355$ s

i) $t = 4705$ s j) $t = 5055$ s k) $t = 5355$ s l) $t = 6000$ s

B) Interface oscillations in r–z plane at $\theta = 0$ and 180 deg

Fig. 4 Three-dimensional bubble deformations in response to combined gravity gradient and g-jitter dominated by g-jitter forces.

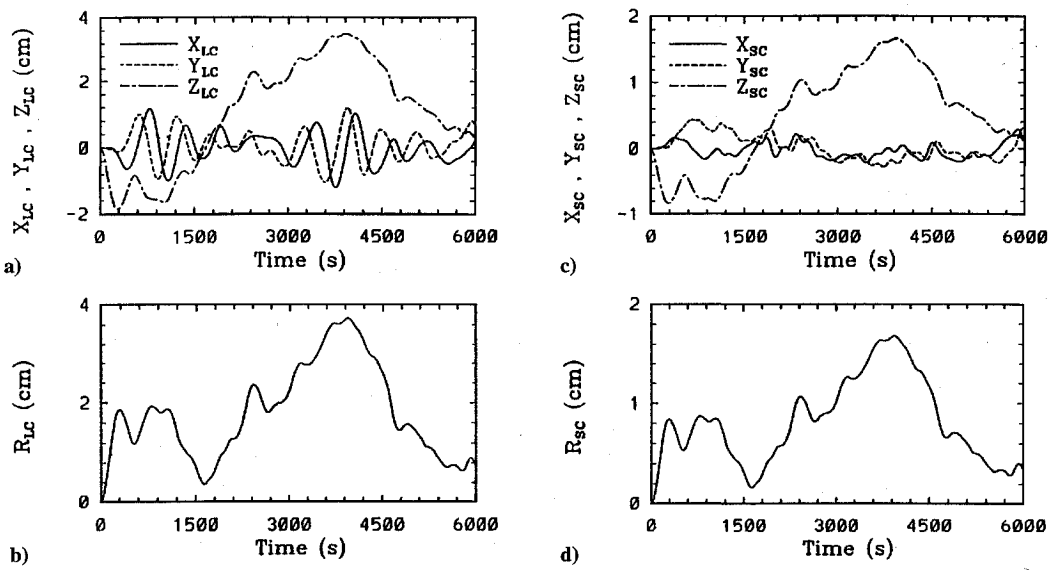

Fig. 5 Time evolution of fluid and spacecraft mass-center fluctuations driven by g-jitter-dominated forces: a) fluid mass center in (x, y, z) components (rotating frame), b) fluid mass center (absolute value), c) spacecraft mass center in (X, Y, Z) components (nonrotating frame), and d) spacecraft mass center (absolute value).

1) $\Delta M_{Lx} > \Delta M_{Ly} \gg \Delta M_{Lz}$ and $|M_{Lx}| > |M_{Ly}| \gg |M_{Lz}|$. This means that the major slosh reaction torques exerted on the Dewar by the fluids in response to the lateral impulse acting on the spacecraft are in the x–y plane in the rotating frame.

2) Similarly to the slosh reaction force, there is a very small time lag (about 10^{-3} s) between the peak of the slosh reaction torque and that of the lateral impulsive torque M_y acting on the spacecraft. In other words, the pattern of M_{Ly} in the first 0.05 s is almost a duplication of that of the impulsive torque acting on the spacecraft with a negative sign, except that the amplitude of the slosh reaction torque is smaller than that of the input because of the damping effect of the fluid system. Also, there is no M_{Lx} or M_{Lz} component of the slosh reaction torque acting on the Dewar during the first 0.05 s. Figure 3d shows the time dependence of the absolute value of the slosh reaction torque acting on the Dewar.

Sloshing Driven by Combined Gravity Gradient and g-Jitter Dominated by g-Jitter Forces

In this subsection, combined gravity gradient and g-jitter with an amplitude of $10^{-6}g_0$ are considered. It is shown in Part 1 (Ref. 8) that gravity gradient accelerations are on the order of $10^{-7}g_0$ for an orbit with an altitude of 650 km. With a background gravity of $10^{-6}g_0$ for g-jitter acceleration as considered in this case, the combined gravity gradient and g-jitter accelerations acting on the spacecraft correspond to the case of orbital accelerations dominated by g-jitter forces acting on the fluid system of the spacecraft. It has been shown that the magnitude of g-jitter accelerations ranges from 10^{-5} to $10^{-9}g_0$.

The characteristics of gravity gradient and g-jitter forces acting on the fluid elements in the rotating Dewar are quite different. Part 1 (Ref. 8) shows that for gravity gradient forces there are greater positive components of acceleration along the direction from the spacecraft mass's center to the Earth's center, and smaller negative components of acceleration transverse to that direction. This phenomenon shows that gravity gradient acceleration exerted on the fluid system of spacecraft is equivalent to the combination of a time-dependent twisting force with a turnaround torsional moment acting on the Dewar when the spacecraft is orbiting the Earth.[10–13] This study shows that for sloshing driven by combined gravity gradient and g-jitter forces, the dynamics are dominated by the g-jitter effects.

Figure 4A shows the time evolution of the three-dimensional dynamical behavior of interface oscillations driven by combined gravity gradient and g-jitter accelerations dominated by the g-jitter force with a low, 0.1-Hz jitter frequency. The g-jitter acceleration, shown in Fig. 3C of Part 1 (Ref. 8), displays a sinusoidal oscillation along the direction from the spacecraft mass's center to the Earth's center [parallel to the unit vector $\boldsymbol{r}_c$ shown in Fig. 3A of Part 1 (Ref. 8)]. These phenomena show that the g-jitter acceleration exerted on the fluid system of the spacecraft is equivalent to oscillatory forces that push the bubble not only upward and downward [see the z component of the g-jitter acceleration shown in Fig. 3C of Part 1 (Ref. 8)], but also leftward and rightward (see the x and y components) as the bubble rotates with respect to the spacecraft spin axis. The time variations of the x and y components of the g-jitter accelerations, shown in Fig. 3C of Part 1 (Ref. 8), correspond to the leftward and rightward oscillations of bubbles shown here in Figs. 4A and 4B. Figure 4B shows the time sequence of the liquid–vapor interface profiles in the vertical r–z plane at $\theta = 0$ and 180 deg. For the various frequencies of g-jitter-dominated accelerations considered, it shows that lower-frequency g-jitter accelerations contribute more to the driving of asymmetric profiles of the interface than do higher-frequency accelerations.[15,16]

Figure 5a shows sloshing due to the time evolution of fluid mass-center fluctuations (in the rotating frame) driven by g-jitter-dominated accelerations coupled with attitude dynamics. The maximum and minimum coordinates of the fluid mass-center fluctuations are $\text{Max}(x_{LC}, y_{LC}, z_{LC}) = (1.19, 1.21, 3.53)$ cm and $\text{Min}(x_{LC}, y_{LC}, z_{LC}) = (-1.20, -1.03, -1.84)$ cm, respectively, and their amplitudes are $\text{Max}(\Delta x_{LC}, \Delta y_{LC}, \Delta z_{LC}) = (2.38, 2.24, 5.37)$ cm. We see that $\Delta z_{LC} > \Delta x_{LC} > \Delta y_{LC}$.

The results on the fluid mass-center fluctuations driven by g-jitter-dominated acceleration coupled with attitude dynamics can be summarized as follows:

1) The oscillations along the x and y directions basically follow the trends of the time dependence of g-jitter accelerations along the x and y axes coupled with attitude dynamics, as shown in Figs. 3C(a) and 3C(b) of Part 1 (Ref. 8).

2) There are fluid mass-center fluctuations with greater amplitude along the z axis in response to the trend of time evolution of g-jitter acceleration along the z axis, in which half of the orbital period is in the positive and the other half in the negative direction. This result is exactly reflected in fluid mass-center fluctuations along the z axis as shown in Fig. 5a with small ripples imposed by the slosh dynamics.

3) Coupling between slosh and attitude dynamics also results in asymmetry of the fluid mass-center fluctuations while the spacecraft is orbiting the Earth.

4) There is a time lag of 150 s between the moment when g-jitter-dominated accelerations act on the spacecraft and the time at which the fluid mass-center fluctuations reach their maximum. Thus, the fluid mass-center fluctuations react rather slowly and do

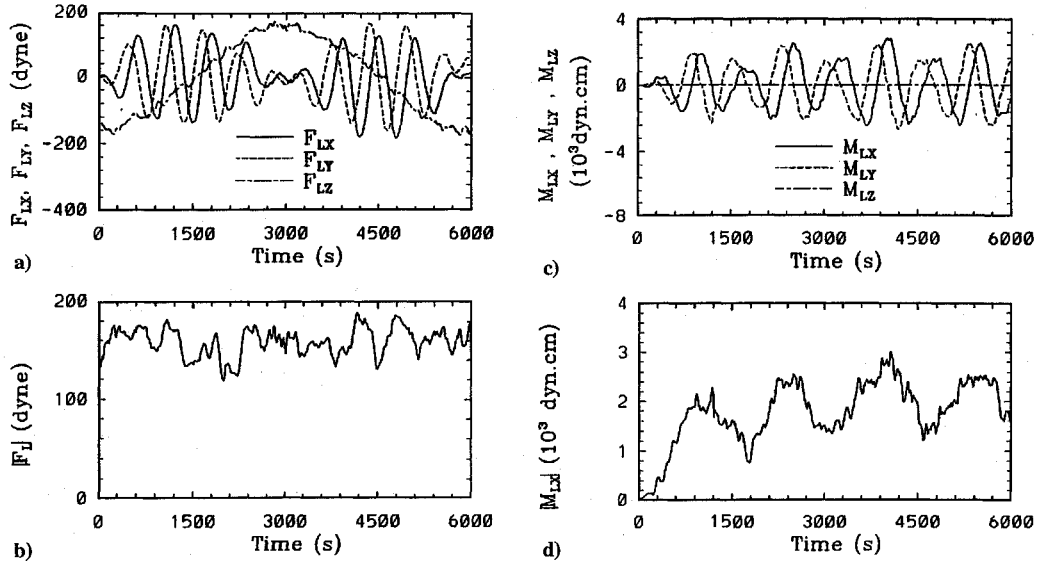

Fig. 6 Time evolution of slosh reaction force and torque (rotating frame) driven by g-jitter-dominated forces: a) slosh reaction force in (x, y, z) components, b) absolute value of slosh reaction torque, c) slosh reaction torque in (x, y, z) components, and d) absolute value of slosh reaction torque.

not instantly change direction at the moment of the direction change of the g-jitter.

5) Figure 5b shows the time dependence of the absolute value of the fluid mass-center fluctuations resulting from the coupling between slosh and attitude dynamics. It shows time-dependent fluctuations with large amplitudes corresponding to directional change of g-jitter with respect to azimuth, while small ripples are imposed on the oscillations by the slosh dynamics.

Spacecraft system mass-center fluctuations (in the nonrotating frame) in response to the coupling between slosh dynamics driven by g-jitter-dominated force and attitude dynamics deviated from normal operation have been studied and are illustrated in Fig. 5c. The values of the maximum and minimum coordinates of the spacecraft mass-center fluctuations are $\text{Max}(X_{SC}, Y_{SC}, Z_{SC}) = (0.29, 0.43, 1.6)$ cm and $\text{Min}(X_{SC}, Y_{SC}, Z_{SC}) = (-0.21, -0.21. - 0.83)$ cm, respectively, and the amplitudes of the spacecraft mass-center fluctuations are $\text{Max}(\Delta X_{SC}, \Delta Y_{SC}, \Delta Z_{SC}) = (0.5, 0.7, 2.5)$ cm. We see that $\Delta Z_{SC} > \Delta Y_{SC} > \Delta X_{SC}$ in the nonrotating frame. Not considering the effect of slosh dynamics on the spacecraft may lead to the wrong results for the case of g-jitter-dominated accelerations.

In this study, characteristics of the slosh reaction force and torque fluctuations exerted on the Dewar in response to the combined gravity gradient and g-jitter accelerations dominated by g-jitter force coupled with attitude dynamics are investigated. With reference to slosh dynamics driven by combined orbital accelerations[10,11] and with the use of mathematical formulations,[8,12,15,16] one can calculate the slosh reaction force and the associated torque acting on the Dewar.

Figure 6a shows the computed time variation of the fluctuations of the slosh reaction force (in the rotating frame) exerted on the Dewar in response to the combined gravity gradient and g-jitter accelerations dominated by g-jitter forces coupled with attitude dynamics. This figure shows the following results:

1) The values of the slosh reaction force fluctuations are $(\Delta F_{Lx}, \Delta F_{Ly}, \Delta F_{Lz}) = (347, 327, 352)$ dynes, so that $\Delta F_{Lz} > \Delta F_{Lx} > \Delta F_{Ly}$, which coincides with the tendency of the fluid mass-center fluctuations, $\Delta z_{Lc} > \Delta x_{Lc} > \Delta y_{Lc}$. The maximum absolute values of the slosh reaction force are $\text{Max}(|F_{Lx}|, |F_{Ly}|, |F_{Lz}|) = (177, 168, 180)$ dynes, so that we also have $|F_{Lz}| > |F_{Lx}| > |F_{Ly}|$.

2) There is a correspondence of tendency between fluid mass-center fluctuations and the slosh reaction force in the x–y plane, as shown in Figs. 5a and 6a.

3) Comparison between Figs. 5a and 6a for the component along the z axis, and also between Figs. 3C(c) [in Part 1 (Ref. 8)] and 5a for the component along the same z axis, shows that the g-jitter-dominated force as a driver and the fluid reaction force as a driven are basically the same. However, it also shows that there is a lag of 150 s between the time of driving-force action and the time of fluid mass motion reacting to the force. In other words, there is an immediate relation between the g-jitter-dominated force exerted on the Dewar and the slosh reaction force acting on the container, but it takes 150 s for the fluid mass motion to change from negative to positive, or vice versa, after the driving force acting on the fluid changes in the same direction.

4) There is no damping effect observed for the slosh reaction force acting on the Dewar in response to the combined gravity gradient and g-jitter forces acting on the fluid one after another during the spacecraft orbital motion, as shown in both Figs. 6a and 6b.

Figure 6c shows time variations of the slosh reaction torque (in the rotating frame) exerted on the Dewar in response to g-jitter-dominated accelerations coupled with attitude dynamics acting on the spacecraft. The values of the slosh reaction torque fluctuations are $(\Delta M_{Lx}, \Delta M_{Ly}, \Delta M_{Lz}) = (5.29, 5.15, 10^{-3}) \times 10^3$ dyne · cm, and the maximum absolute values of the slosh reaction torque are $\text{Max}(|M_{Lx}|, |M_{Ly}|, |M_{Lz}|) = (2.85, 2.64, 10^{-3}) \times 10^3$ dyne · cm. This figure shows the following results:

1) $\Delta M_{Lx} > \Delta M_{Ly} \gg \Delta M_{Lz}$ and $|M_{Lx}| > |M_{Ly}| \gg |M_{Lz}|$. This means that the major slosh reaction torques exerted by the fluid on the Dewar in the rotating frame are in the x–y plane in response to the g-jitter-dominated accelerations acting on the spacecraft.

2) The sinusoidal oscillations of M_{Lx} and M_{Ly} resemble the time variation of the azimuth angle for the spacecraft orbital motion. For the purpose of easier comparison between the slosh reaction torques in the rotating and nonrotating frames, Fig. 6d shows the time variation of the absolute value of the slosh reaction torque acting on the Dewar.

Coupling of Attitude and Slosh Dynamics

A mathematical formulation of spacecraft attitude dynamics—that of a rigid body with six degrees of freedom, three being translational and three rotational—has been presented in Part 1 (Ref. 8). In this study, our primary interest is to investigate slosh dynamics driven by environmental disturbances coupled with attitude dynamics. In other words, we investigate how additional accelerations (moments) produced by slosh reaction forces (torques) may cause a spacecraft to deviate from normal operation in terms of displacement, velocity, acceleration, and angular momentum. As shown in Part 1 (Ref. 8), inertial frames are adopted for the translational equations, and Eulerian angles are used for the three rotational equations.[17] As usual, ψ, θ, and ϕ are defined as the heading, attitude, and bank angles,[17] which are illustrated in Fig. 7a.

In this study, computations of spacecraft dynamical parameters deviating from those in normal operation have been carried out. These deviations result from the spacecraft attitude behavior due to the action of environmental disturbances on spacecraft systems in which there is coupling between slosh and attitude dynamics. These results are derived with and without the assumption of closed-loop attitude control.

Spacecraft Dynamics Driven by a Lateral Impulse

Figure 7b shows the time dependence of the Eulerian angles (θ, ψ, ϕ). It shows that there is a sinusoidal variation of θ and ψ, but a linear variation of ϕ, which is associated with the angle of rotation about the z axis. Figure 7c shows a sketch of corresponding time variations of the trace of the spacecraft rotation axis. The time variations of the angle in degrees between the initial position and the direction of the spacecraft rotation axis at times represented by numbers in Fig. 7c are listed. This shows that the spacecraft spin axis is coning under the influence of coupling between the slosh dynamics driven by a lateral impulse and the deviation of the attitude dynamics from normal operation. This figure indicates that the spacecraft is unlikely to return to its original attitude without correction once any external force, such as the lateral impulse, has been applied to the spacecraft.

Figure 7d shows fluid angular momentum fluctuations in the rotating frame. It shows a sinusoidal oscillation in the components along the x and y axes, while a relatively small fluctuation appears in the component along the z axis. The values of the angular momentum fluctuations are $(\Delta H_x, \Delta H_y, \Delta H_z) = (9.6, 10.7, 1.7) \times 10^5$ g · cm^2/s, and the maximum absolute values of the fluid angular momentum are $\text{Max}(|H_x|, |H_y|, |H_z|) = (5.0, 5.3, 0.9) \times 10^5$ g · cm^2/s. Thus $\Delta H_y > \Delta H_x \gg \Delta H_z$ and $|H_y| > |H_x| \gg |H_z|$ in the rotating frame. This is due to the fact that the major contributing torque of the impulse is applied about the y axis and is transferred to the x axis through the Coriolis force in the rotating frame.

Spacecraft system mass-center fluctuations (in the nonrotating frame) in response to the coupling between slosh dynamics driven by a lateral impulse and the deviation of the attitude dynamics from normal operation have been studied and are illustrated in Fig. 2c. The values of the maximum and minimum coordinates of spacecraft mass-center fluctuations are $\text{Max}(X_{SC}, Y_{SC}, Z_{SC}) = (0.85, 0.63, -0.24)$ cm and $\text{Min}(X_{SC}, Y_{SC}, Z_{SC}) = (-0.6, -0.76, -0.50)$ cm, respectively, and the fluctuations of the maximum spacecraft mass-center disturbances are $\text{Max}(\Delta X_{SC}, \Delta Y_{SC}, \Delta Z_{SC}) = (1.46, 1.39, 0.26)$ cm. Thus $\Delta X_{SC} > \Delta Y_{SC} > \Delta Z_{SC}$ in the nonrotating frame. Results for the spacecraft mass-center fluctuations in response to coupling between slosh dynamics driven by impulse and the deviation of the attitude dynamics from normal operation are very similar to those derived from the fluid mass-center fluctuations obtained earlier, except that 1) the former case is in the nonrotating frame and the latter is in the rotating frame, in which the Coriolis force transfers disturbance from the X to the Y axis; and 2) the former case yields smaller magnitudes of fluctuations because of the averaging between the dry mass of the spacecraft and the fluid mass fluctuations. Figure 2d shows the time dependence of the absolute value of spacecraft system mass-center fluctuations. Comparison between Figs. 2b and 2d shows that spacecraft mass-center fluctuations are dominated by the fluid system mass-center fluctuations. Not considering the effect of slosh dynamics acting on the spacecraft may lead to the wrong results for the motion after the vanishing of the lateral impulse.

During the coupling between slosh dynamics driven by an impulse and the spacecraft attitude dynamics, the total force (F_{Si}) and torque (M_{Si}) acting on the spacecraft are $F_{Si} = F_{Li} + F_{Di}$ and $M_{Si} = M_{Li} + M_{Di}$, to be computed from the coupling of the attitude dynamics (translational and rotational equations) and the slosh dynamics (fluid equations). Figure 8a shows the computed time variation of the fluctuations of total force (in the nonrotating frame) exerted on the spacecraft as a result of coupling between sloshing and attitude dynamics. This figure shows the following results:

1) The values of the total force fluctuations acting on the spacecraft are $(\Delta F_{SX}, \Delta F_{SY}, \Delta F_{SZ}) = (323, 306, 41.2)$ dynes, so that

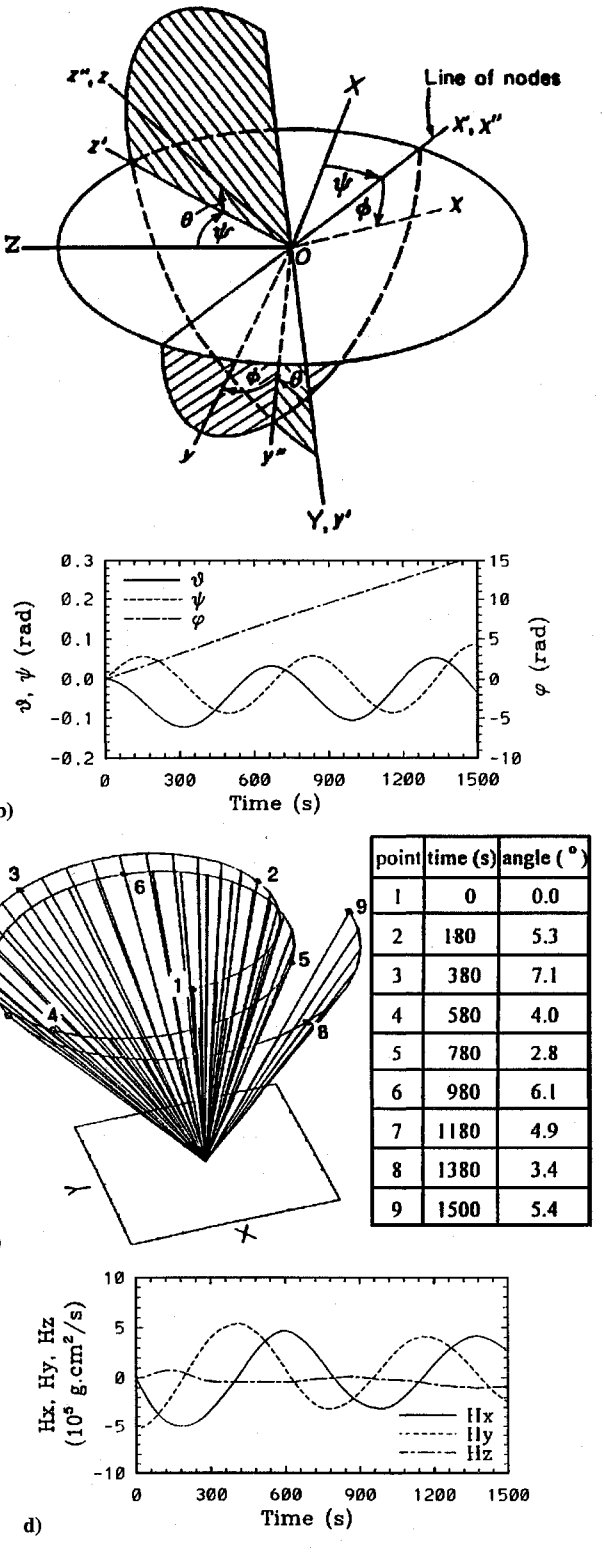

point	time (s)	angle (°)
1	0	0.0
2	180	5.3
3	380	7.1
4	580	4.0
5	780	2.8
6	980	6.1
7	1180	4.9
8	1380	3.4
9	1500	5.4

Fig. 7 Parameters in spacecraft orbital dynamics driven by lateral impulse: a) coordinates and Eulerian angles, b) time evolution of Eulerian angles, c) time evolution of the trace of the spacecraft rotation axis, and d) time evolution of fluid angular momentum fluctuations (rotating frame).

$\Delta F_{SX} > \Delta F_{SY} > \Delta F_{SZ}$ in the nonrotating frame. The maximum absolute values of the total force acting on the spacecraft are $\text{Max}(|F_{SX}|, |F_{SY}|, |F_{SZ}|) = (189, 154, 21)$ dynes. Thus we also have $|F_{SX}| > |F_{SY}| > |F_{SZ}|$, which coincides with the tendency of the spacecraft mass-center fluctuations $(\Delta X_{SC} > \Delta Y_{SC} > \Delta Z_{SC})$ in the nonrotating frame.

2) F_{Li} in the rotating frame and F_{Si} in the nonrotating frame are very hard to compare. Figure 8b shows the time variation of the

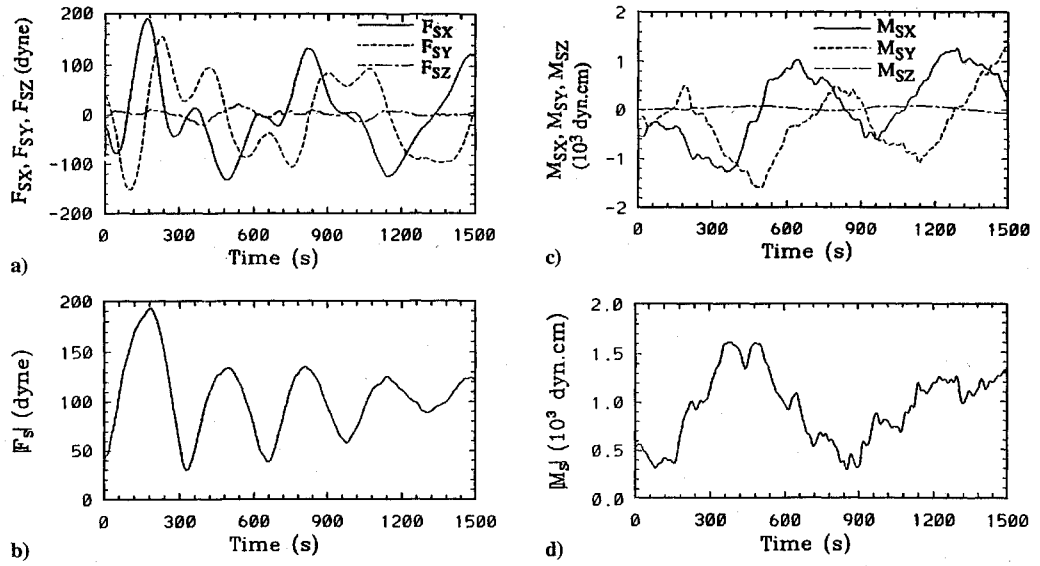

Fig. 8 Time evolution of total force and torque acting on spacecraft (nonrotating frame) driven by lateral impulse: a) total force in (X, Y, Z) components, b) absolute value of total force, c) total torque in (X, Y, Z) components, and d) absolute value of total torque.

absolute values of the total force acting on the spacecraft. Comparison between Figs. 3b and 8b shows that $|F_S|$ and $|F_L|$ are basically the same, with a time lag of 10^{-3} s after the vanishing of the lateral impulse. This result implies that the total force acting on the spacecraft is dominated by a slosh reaction force contributed by the fluid system. Not considering the effect of the slosh reaction force may lead to the wrong results for the motion after the vanishing of the lateral impulse. There is a very small time lag (about 10^{-3} s delay) between the time the force acts on the Dewar and time it is transferred from the Dewar to become a reactive force acting on the fluid. This time lag between action and reaction is quite different from the time for shifting the spacecraft mass-center fluctuations; the latter reaches a maximum value at time $t = 150$ s, that is, 150 s after the time the impulse acts on the Dewar and the reaction force acts on the fluid.

4) The damping effect of the total force acting on the spacecraft resulting from the coupling between slosh and attitude dynamics is shown in Figs. 8a and 8b. The figures show that the fluid acts as an oscillating damper in response to the coupling between sloshing and attitude dynamics after the vanishing of the lateral impulse acting on the fluid system.

Figure 8c shows the time variation of the total torque (in the nonrotating frame) exerted on the spacecraft resulting from the coupling between sloshing and attitude dynamics. The values of the total torque fluctuations acting on the spacecraft are $(\Delta M_{SX}, \Delta M_{SY}, \Delta M_{SZ}) = (2.53, 2.88, 0.1) \times 10^3$ dyne · cm, and the maximum absolute values of the total torque acting on the spacecraft are $\text{Max}(|M_{SX}|, |M_{SY}|, |M_{SZ}) = (1.27, 1.59, 10^{-2}) \times 10^3$ dyne · cm in the nonrotating frame. This figure shows the following results:

1) $\Delta M_{SY} > \Delta M_{SX} \gg \Delta M_{SZ}$ and $|M_{SY}| > |M_{SX}| \gg |M_{SZ}|$. This means that the major torques exerted on the spacecraft in the nonrotating frame are in the X–Y plane and result from coupling between sloshing and orbital dynamics after the vanishing of the impulse.

2) There is also a very small time lag (about 10^{-3} s) between the time of action and the time of reaction for a torque acting between the spacecraft and the fluid.

3) Figure 8d shows the time variation of the absolute value of total torque acting on the spacecraft resulting from the coupling between sloshing and attitude dynamics. Comparison between Figs. 3d and 8d shows that $|M_S|$ and $|M_L|$ are basically the same, with a time lag of 10^{-3} s after the vanishing of the impulse torque. This result also implies that the total torque acting on the spacecraft is dominated by the slosh reaction torque contributed by the fluid system. Not considering the effect of the slosh reaction torque acting on the spacecraft may lead to the wrong results for the motion after the vanishing of the impulse torque.

4) The damping effect of the total torque acting on the spacecraft resulting from the coupling of sloshing and attitude dynamics is shown in Figs. 8c and 8d.

The time dependence of the spacecraft angular velocity in the rotating frame, and the spacecraft translational displacement, velocity, and acceleration in the nonrotating frame, which deviate from normal spacecraft operation because of coupling between slosh and attitude dynamics, have been calculated and are plotted in Figs. 9a, 9b, 9c, and 9d, respectively. Figure 9a shows the time evolution of $(\omega_x, \omega_y, \omega_z)$ in the rotating frame. It shows that ω_x and ω_y fluctuate in the ranges $(8.1, 10^{-3}) \times 10^{-3}$ and $(6.6, 10^{-3}) \times 10^{-3}$ rad/s, respectively, while ω_z is relatively constant with a value of 1.05×10^{-2} rad/s and fluctuation of 10^{-7} rad/s in the rotating frame.

Figure 9b shows the time evolution of the spacecraft translational displacement (in the nonrotating frame), which deviates from normal spacecraft operation, in response to an impulse ending at $t = 10^{-2}$ s. As the impulse is acting along the X axis, there is a time-dependent incremental displacement along the X axis, deviating from the normal operation, with sinusoidal oscillations affected by slosh dynamics, while the displacements along the Y and Z axes are relatively small, with fluctuations in the ranges of $(8.1, -4.0)$ and $(5.0, -0.1)$ cm, respectively, after the vanishing of impulse at $t = 10^{-2}$ s.

Figure 9c shows the time evolution of the spacecraft translational velocity (in the nonrotating frame), deviating from normal spacecraft operation, in response to the impulse ending at $t = 10^{-2}$ s. It shows that the major translational velocities are V_X and V_Y with fluctuations in the ranges $(6.8, 0.14) \times 10^{-2}$ and $(3.7, -3.4) \times 10^{-2}$ cm/s, respectively, while V_Z is relatively small, with the range $(6.3, -1.5) \times 10^{-3}$ cm/s. The sinusoidal oscillations of spacecraft translational velocities deviating from normal operation are due to the effect of sloshing dynamics from the fluid system.

Figure 9d shows the time evolution of the spacecraft translational acceleration (in the nonrotating frame), deviating from normal spacecraft operation, in response to an impulse ending at $t = 10^{-2}$ s. Similarly to the translational velocities, the major translational accelerations are a_X and a_Y with fluctuations in the ranges $(5.4, -3.8) \times 10^{-4}$ and $(4.4, -4.3) \times 10^{-4}$ cm/s^2, respectively, while a_Z is relatively small with the range $(5.9, -5.8) \times 10^{-5}$ cm/s^2. Again, sinusoidal oscillations of the spacecraft translational accelerations deviating from normal operation are due to the effect of slosh dynamics from the fluid system. This shows the effect of slosh dynamics on the deviation of spacecraft translational displacement, velocity, and acceleration from normal operation.

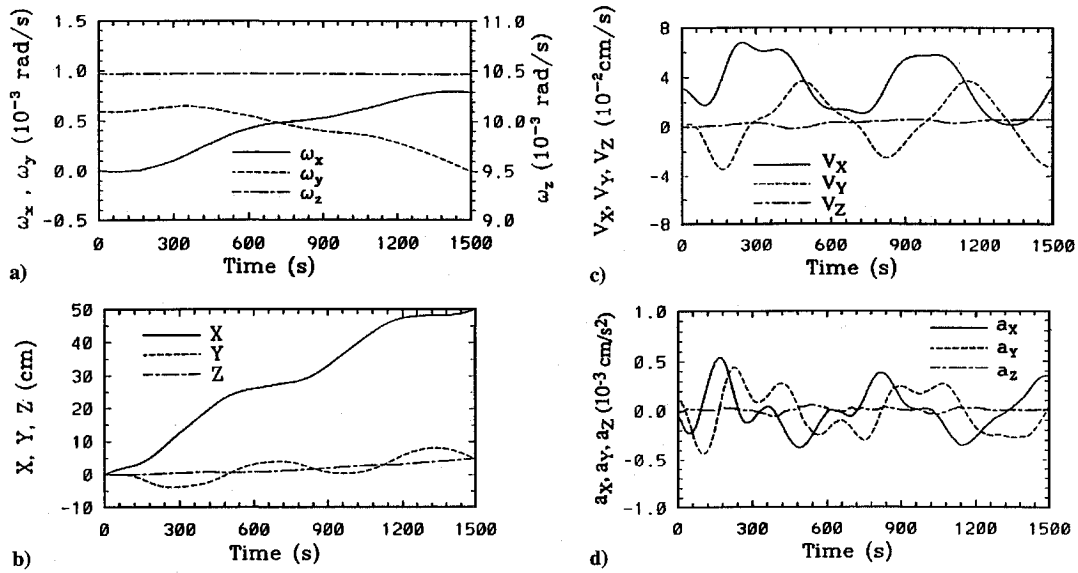

Fig. 9 Time evolution of spacecraft attitude dynamics parameters driven by lateral impulse: a) angular velocities (rotating frame), b) translational displacements (nonrotating frame), c) translational velocities (nonrotating frame), and d) translational accelerations (nonrotating frame).

Spacecraft Dynamics Driven by Combined Gravity Gradient and *g*-Jitter and Dominated by *g*-Jitter Forces

Figure 10a shows the time dependence of the Eulerian angles (θ, ψ, ϕ). It shows that there is a sinusoidal variation for θ and ψ but a linear variation for ϕ, which is associated with the spin angle about the rotation axis z.

Figure 10b shows a sketch of the corresponding time variation of the trace of the spacecraft spin axis. The time variations of the angle in degrees between the initial position and the direction of the spacecraft spin axis at times represented by numbers in Fig. 10b are listed. This shows that the spacecraft spin axis is coning with large and small swings under the influence of coupling between the slosh dynamics driven by g-jitter-dominated forces and the deviation of the attitude dynamics from normal operation. This spin-axis coning with large and small swings is mainly driven by coupling of sloshing and attitude dynamics during the time while the azimuth angle of the spin axis is passing through zero. This figure indicates that a spacecraft is unlikely to return to its original attitude without correction once any external force, such as a g-jitter force, has been applied to the spacecraft.

Figure 10c shows fluid angular momentum fluctuations in the rotating frame. It shows a sinusoidal oscillation of the components along the x and y axis while a relatively small fluctuation appears in the component along the z axis. The values of the angular momentum fluctuations are $(\Delta H_x, \Delta H_y, \Delta H_z) = (3.6, 3.7, 0.83) \times 10^6$ g · cm²/s, and the maximum absolute values of the fluid angular momentum are $\text{Max}(|H_x|, |H_y|, |H_z|) = (1.8, 1.9, 0.76) \times 10^6$ g · cm²/s. Thus $\Delta H_y > \Delta H_x \gg \Delta H_z$ and $|H_y| > |H_x| \gg |H_z|$ in the rotating frame. This is because the major contributing slosh reaction torques are acting in the x–y plane in the rotating frame.

The spacecraft system mass-center fluctuations (in the nonrotating frame) in response to the coupling between slosh dynamics driven by g-jitter-dominated force and attitude dynamics deviating from normal operation have been studied and are illustrated in Fig. 5c. The values of the maximum and minimum of coordinates of the spacecraft mass-center fluctuations are $\text{Max}(X_{SC}, Y_{SC}, Z_{SC}) = (0.29, 0.43, 1.6)$ cm and $\text{Min}(X_{SC}, Y_{SC}, Z_{SC}) = (-0.21, -0.27, -0.83)$ cm, respectively, and the fluctuations of the maximum spacecraft mass-center disturbances are $\text{Max}(\Delta X_{SC}, \Delta Y_{SC}, \Delta Z_{SC}) = (0.5, 0.7, 2.5)$ cm. We see that $\Delta Z_{SC} > \Delta Y_{SC} > \Delta X_{SC}$ in the nonrotating frame. The results for the spacecraft mass-center fluctuations in response to coupling between slosh dynamics driven by g-jitter-dominated forces and orbital dynamics deviating from normal operation are very similar to those for the fluid mass-center fluctuations obtained earlier except that 1) the former case is in the nonrotating frame, and the

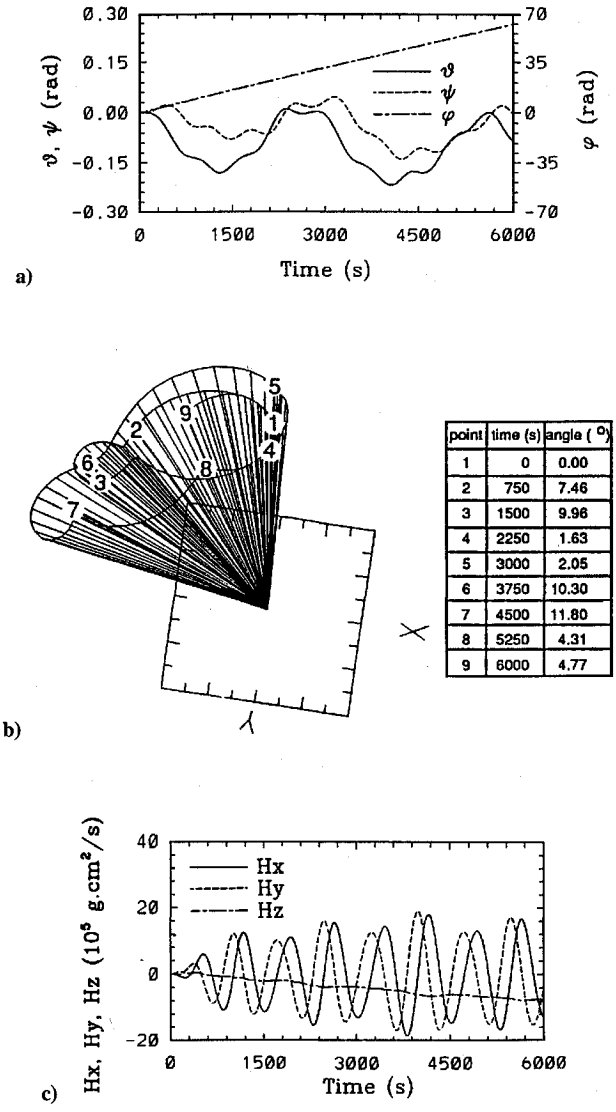

point	time (s)	angle (°)
1	0	0.00
2	750	7.46
3	1500	9.96
4	2250	1.63
5	3000	2.05
6	3750	10.30
7	4500	11.80
8	5250	4.31
9	6000	4.77

Fig. 10 Parameters in spacecraft attitude dynamics driven by *g*-jitter-dominated forces: a) time evolution of Eulerian angles, b) time evolution of the trace of spacecraft rotation axis, and c) time evolution of fluid angular momentum fluctuations (rotating frame).

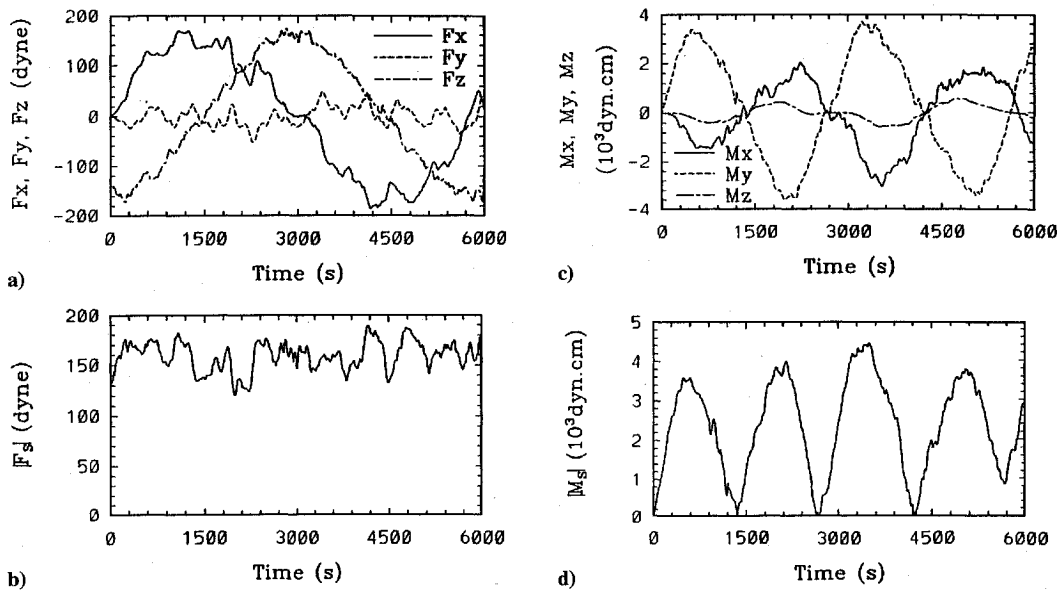

Fig. 11 Time evolution of total force and torque acting on spacecraft (nonrotating frame) driven by g-jitter-dominated forces: a) total force in (X, Y, Z) components, b) absolute value of total force, c) total torque in (X, Y, Z) components, and d) absolute value of total torque.

latter is in the rotating frame and 2) the former case yields smaller magnitudes of fluctuations because of the averaging between the dry mass of the spacecraft and the fluid mass fluctuations. Figure 5d shows the time variation of the absolute value of the spacecraft system mass-center fluctuations. Comparison between Figs. 5b and 5d shows that spacecraft mass-center fluctuations are dominated by the fluid system mass-center fluctuations. Not considering the effect of slosh dynamics acting on the spacecraft may lead to the wrong results when g-jitter-dominated acceleration acts on the orbiting spacecraft.

During the coupling between slosh dynamics driven by g-jitter-dominated forces and spacecraft attitude dynamics, the total forces (F_{Si}) and torque (M_{Si}) acting on the spacecraft are $F_{si} = F_{Li} + F_{Di}$ and $M_{Si} = M_{Li} + M_{Di}$, to be computed from coupling of attitude dynamics (translational and rotational equations) and slosh dynamics (fluid equations). Figure 11a shows the computed time variation of the fluctuations of the total force (in the nonrotating frame) on the spacecraft resulting from coupling between sloshing and attitude dynamics. This figure shows the following results:

1) The values of the total force fluctuations acting on the spacecraft are $(\Delta F_{SX}, \Delta F_{SY}, \Delta F_{SZ} = (359, 102, 352)$ dynes, so that $\Delta F_{SX} > \Delta F_{SZ} > \Delta F_{SY}$ in the nonrotating frame. The maximum absolute values of the total force acting on the spacecraft are $\text{Max}(|F_{SX}|, |F_{SY}|, |F_{SZ}) = (185, 52, 177)$ dynes. Thus also $|F_{SX}| > |F_{SZ}| > |F_{SY}|$, which does not coincide with the tendency of the spacecraft mass-center fluctuations, $\Delta Z_{SC} > \Delta Y_{SC} > \Delta X_{SC}$ in the nonrotating frame. This is because constantly fluctuating g-jitter-dominated accelerations [see Fig. 3 in Part 1 (Ref. 8)] acting on the fluid element do not provide enough time for the fluid to react before the arrival of the next such acceleration. This causes a mismatch between the actuating force and the fluid displacement.

2) F_{Li} in the rotating frame and F_{Si} in the nonrotating frame are very hard to compare. Figure 11b shows the time variation of the absolute values of total force acting on the spacecraft.

Comparison between Figs. 6b and 11b shows that $|F_S|$ and $|F_L|$ are basically the same. This is due to the following:

1) The fluid is constantly moving because of the bubble deformations driven by the g-jitter-dominated accelerations, which contributes to the time evolution of the slosh reaction forces shown in Fig. 6b.

2) Geometrically and dynamically, the solid-body portion of the spacecraft is basically a rigid body and symmetric about the rotation axis. This implies that the total force acting on the solid-body portion of the spacecraft induced by the g-jitter-dominated accelerations is zero at all times.

3) Addition of items 1 and 2 shows that the total contribution of forces acting on the spacecraft diven by g-jitter-dominated acceleration is just the total force contributed by the fluid system. Not considering the effect of the slosh reaction force acting on the spacecraft may lead to the wrong results.

4) There is no damping effect shown for the total force acting on the spacecraft resulting from the coupling between slosh and attitude dynamics, because the g-jitter-dominated force is equivalent to up-and-down and leftward-and-rightward forces acting on the fluid system one after another, as shown in both Figs. 11a and 11b.

Figure 11c shows the time variation of the total torque (in the nonrotating frame) on the spacecraft resulting from the coupling between sloshing and attitude dynamics. The values of the total torque fluctutions acting on the spacecraft are $(\Delta M_{SX}, \Delta M_{SY}, \Delta M_{SZ}) = (5.1, 7.3, 1.1) \times 10^3$ dyne · cm, and the maximum absolute values of the total torque acting on the spacecraft are $\text{Max}(|M_{SX}|, |M_{SY}|, |M_{SZ}|) = (3.0, 3.7, 0.57) \times 10^3$ dyne · cm in the nonrotating frame. This figure shows the following results:

a) $\Delta M_{SY} > \Delta M_{SX} \gg \Delta M_{SZ}$ and $|M_{SY}| > |M_{SX}| \gg |M_{SZ}|$. This means that the major torques exerted on the spacecraft in the nonrotating frame are in the x–y plane and result from coupling between sloshing and attitude dynamics.

b) Figure 8d shows the time variation of the absolute value of the total torque acting on the spacecraft resulting from the coupling between sloshing and attitude dynamics. Comparison between Figs. 6d and 11d shows that there is a basic difference between $|M_S|$ and $|M_L|$. This is for the following reasons. 1) Comparison between Figs. 6b and 11b shows that there is no difference between $|F_S|$ and $|F_L|$, because the total force on the solid-body portion of the spacecraft induced by the g-jitter-dominated acceleration is zero. 2) The zero resultant force leads to a nonzero moment acting on the spacecraft because of the additional force couple due to the nonzero moment arm. 3) Addition of the torque contributed by the slosh reaction from the fluid and the nonzero force couple from solid-body portion of spacecraft yields a time evolution of the total torque shown in Fig. 11d, which is different from the contribution made by the slosh reaction alone. 4) The four major peaks shown in Figs. 6d and 11d are due to the direction change of the spacecraft rotation axis with respect to the direction of the g-jitter-dominated force—that is, the azimuth angle ψ_E. Namely, the four peaks in the torque result from the change of ψ_E from 0 to $\pi/2$, $\pi/2$ to π, π to $\frac{3}{2}\pi$, and $\frac{3}{2}\pi$ to 2π. 5) Comparison of the magnitudes between Figs. 6d and 11d shows that the major contribution to the total torque acting on the spacecraft is due to slosh reaction. Not considering the effect of the slosh reaction torque acting on the spacecraft may lead to the wrong results.

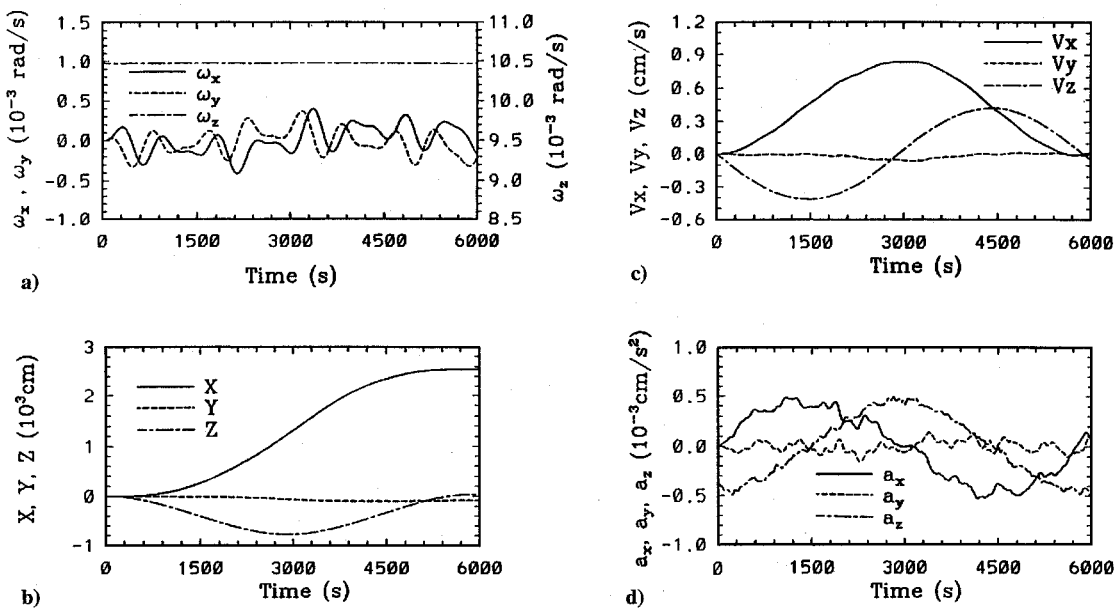

Fig. 12 Time evolution of spacecraft attitude dynamics parameters driven by *g*-jitter-dominated forces: a) angular velocities (rotating frame), b) translational displacements (nonrotating frame), c) translational velocities (nonrotating frame), and d) translational accelerations (nonrotating frame).

c) There is no damping effect shown for the total torque acting on the spacecraft resulting from the coupling of sloshing and attitude dynamics, because *g*-jitter acceleration is just like a time sequence of up-and-down and leftward-and-rightward forces acting on the spacecraft one after another, as has been shown in Figs. 11c and 11d.

The time-dependent spacecraft angular velocity in the rotating frame and spacecraft translational displacement, velocity, and acceleration in the nonrotating frame, deviating from normal spacecraft operation and resulting from coupling between slosh and orbital dynamics, have been calculated and are illustrated in Figs. 12a, 12b, 12c, and 12d, respectively.

Figure 12a shows the time evolution of $(\omega_x, \omega_y, \omega_z)$ in the rotating frame. It shows that ω_x, ω_y fluctuate in the ranges $(3.9, -4.1) \times 10^{-4}$ and $(3.7, -3.2) \times 10^{-4}$ rad/s, respectively, while ω_z is relatively constant with a value of 1.05×10^{-2} rad/s and fluctuation of 10^{-7} rad/s in the rotating frame.

Figure 12b shows the time evolution of the spacecraft translational displacement (in the nonrotating frame), deviating from normal spacecraft operation, in response to the coupling of slosh and attitude dynamics driven by *g*-jitter-dominated accelerations. In the nonrotating frame, the spacecraft orbit is in the X–Z plane, with the direction of the spin axis, $-Z$, constantly pointing toward Rigel for the case of the Gravity Probe-B spacecraft. There is a time-dependent incremental displacement with a maximum value of 2.5×10^3 cm along the X axis, deviating from normal operation, while the displacements along the Y and Z axes are relatively small, with fluctuations in the ranges (0.0, −94) and (38, −772) cm, respectively.

Figure 12c shows the time evolution of the spacecraft translational velocity (in the nonrotating frame), deviating from normal spacecraft operation, in response to the *g*-jitter-dominated forces. It shows that the major translational velocities are V_X and V_Z in the spacecraft orbital plane, with fluctuations in the ranges $(83, -0.5) \times 10^{-2}$ and $(42, -41) \times 10^{-2}$ cm/s, respectively, while V_Y, with direction perpendicular to the orbital plane, is relatively small with a range $(1.6, -6.0) \times 10^{-2}$ cm/s. Sinusoidal oscillations of spacecraft translational velocities deviating from normal operation are due to the effect of sloshing dynamics from the fluid system. Figure 12d shows the time evolution of the spacecraft translational acceleration (in the nonrotating frame), deviating from normal spacecraft operation, in response to *g*-jitter-dominated forces. Similarly to the translational velocities, the major translational accelerations are a_X and a_Z with fluctuations in the ranges $(4.9, -5.3) \times 10^{-4}$ and $(4.9, -4.9) \times 10^{-4}$ cm/s^2, respectively, whereas a_Y is relatively small with the range $(1.4, -1.4) \times 10^{-4}$ cm/s^2. Again, small ripple oscillations of spacecraft translational accelerations deviating from normal operation are due to the effect of slosh dynamics from fluid systems. This example shows the effect of slosh dynamics in causing the spacecraft translational displacement, velocity, and acceleration to deviate from their values in normal operation, the major deviations being produced in the components in the orbital plane.

In this study, characteristics of the orbit environmental disturbances and their effects on slosh dynamics coupled with spacecraft dynamics considered are given in Table 1 of Part 1 (Ref. 8). The considerations of Newtonian fluid applicable to helium II adopted in this paper have been discussed earlier.[1,18,19]

Conclusions

The dynamics of a spinning spacecraft Dewar acted on by orbital environmental disturbances—including lateral impulse, gravity gradient, and *g*-jitter forces—have been studied. The results show that large-amplitude fluctuating slosh reaction forces and torques can be induced that drive the spacecraft out of normal operation.

In this study liquid helium II is considered in the investigation. The assumption of Newtonian fluid is applicable when the fluid velocity of helium II exceeds the critical velocity, which is a function of the fluid temperature and the size of the container. The rotational velocities of liquid helium considered in this paper are far greater than the critical velocities, which assures the validity of the Newtonian fluid assumption. The results obtained in this study are equally applicable to other Newtonian fluids (such as liquid hydrogen, liquid nitrogen, or hydrazine) through the use of similarity parameters (Bond number, Weber number, capillary number, Grashof number, Froude number, Reynolds number, etc.) with nondimensionalized material properties (density, viscosity, surface tension, specific heat, etc.). Detailed discussions of the use of similarity parameters are not repeated here. As to fluids with non-Newtonian properties, the models of slosh reaction forces and torques employed in this study are also applicable provided that the proper adjustment is made to the definition of viscosity based on the ratio of viscous stress to fluid velocity shear, i.e.,

$$\mu = \frac{\tau}{(\partial u/\partial y)^n} \tag{3}$$

where $n = 1$ for Newtonian and $n \neq 1$ for non-Newtonian fluids. Here μ, τ, u, y, and n stand for the viscous coefficient, viscous

stress, fluid velocity, coordinate transverse to the direction of fluid velocity, and proportionality constant. Thus, the models presented in this study are quite general and are equally applicable to both Newtonian and non-Newtonian fluids.

In the study of the behavior of dynamical systems and the development of the associated control systems, a mechanical system, such as the mass–spring–damper system, has frequently been used. This mechanical system is not appropriate to use in the development of control techniques associated with sloshing dynamics, because of the highly nonlinear behavior involved in the fluid mechanics governed by the Navier–Stokes equations. This is why the dynamical model of coupling between slosh and orbital dynamics has been adopted to study the attitude and guidance controls associated with liquid sloshing dynamics.

For the purpose of the study, the slosh dynamics is based on a rotating frame, and the attitude dynamics on a nonrotating frame. Computations of the fluctuations of spacecraft mass center and of the forces and torques acting on the spacecraft and driven by these environmental disturbances indicate that the major contributions of attitude dynamics are those coupled with slosh dynamics. The liquid motions create large-amplitude fluctuations in the slosh reaction forces and torques acting on the Dewar, which drive the spacecraft to deviate from normal operation. In fact, not considering the effect of slosh dynamics on the spacecraft may lead to the wrong results. The asymmetric orientation of the liquid sloshing in the tank may also create control and pointing problems, because the translational displacement, velocity, and acceleration as well as the rotational displacement and velocity deviate from normal spacecraft operation.

Acknowledgments

The authors appreciate the support received from NASA through Grant NAG8-938 and Contract NAS839609/Delivery Order 103.

References

[1]Hung, R. J., and Long, Y. T., "Effect of Baffle on Slosh Reaction Forces in Rotating Liquid Helium Subjected to a Lateral Impulse in Microgravity," *Cryogenics*, Vol. 35, No. 9, 1995, pp. 589–597.

[2]Avduyevsky, V. S. (ed.), *Scientific Foundations of Space Manufacturing*, MIR, Moscow, 1984, p. 450.

[3]Forward, R. L., "Flattening Space-Time Near the Earth," *Physical Review A*, Vol. 26, No. 5, 1982, pp. 735–744.

[4]Misner, C. W., Thorne, K. S., and Wheeler, J. A., *Gravitation*, W. H. Freeman, San Francisco, 1973, pp. 253–674.

[5]Kamotani, Y., Prasad, A., and Ostrach, S., "Thermal Convection in an Enclosure Due to Vibrations Aboard a Spacecraft," *AIAA Journal*, Vol. 19, No. 4, 1981, pp. 511–516.

[6]Hung, R. J., Lee, C. C., and Leslie, F. W., "Spacecraft Dynamical Distribution of Fluid Stresses Activated by Gravity Jitters Induced Slosh Waves," *Journal of Guidance, Control, and Dynamics*, Vol. 15, No. 3, 1992, pp. 817–824.

[7]Hung, R. J., Lee, C. C., and Leslie, F. W., "Similarity Rules in Gravity Jitter-Related Spacecraft Liquid Propellant Slosh Waves Excitation," *Journal of Fluids and Structures*, Vol. 6, No. 3, 1992, pp. 493–522.

[8]Hung, R. J., Long, Y. T., and Chi, Y. M., "Slosh Dynamics Coupled with Spacecraft Attitude Dynamics Part 1: Formulation and Theory," *Journal of Spacecraft and Rockets*, Vol. 33, No. 4, 1996, pp. 575–581.

[9]Hung, R. J., and Long, Y. T., "Response and Decay of Rotating Cryogenic Liquid Reacted to Impulsive Accelerations in Microgravity," *Transactions of the Japan Society for Aeronautical and Space Science*, Vol. 37, No. 2, 1995, pp. 291–310.

[10]Hung, R. J., and Pan, H. L., "Fluid Force Activated Spacecraft Dynamics Driven by Gravity Gradient and Jitter Accelerations," *Journal of Guidance, Control, and Dynamics*, Vol. 18, No. 5, 1995, pp. 1190–1196.

[11]Hung, R. J., and Pan, H. L., "Differences in Gravity Gradient and Gravity Jitter Excited Slosh Waves in Microgravity," *Transactions of the Japan Society for Aeronautical and Space Sciences*, Vol. 36, No. 1, 1993, pp. 153–169.

[12]Hung, R. J., and Pan, H. L., "Gravity Gradient or Gravity Jitter Induced Viscous Stress and Moment Fluctuations in Microgravity," *Fluid Dynamic Research*, Vol. 34, No. 1, 1994, pp. 29–44.

[13]Hung, R. J., Pan, H. L., and Leslie, F. W., "Fluid System Angular Momentum and Moment Fluctuations Gravity Gradient of Gravity Jitter in Microgravity," *Journal of Flight Sciences and Space Research*, Vol. 18, No. 1, 1994, pp. 195–202.

[14]Hung, R. J., and Pan, H. L., "Asymmetric Slosh Wave Excitation in Liquid–Vapor Interface Under Microgravity," *Acta Mechanica Sinica*, Vol. 9, No. 2, 1993, pp. 298–311.

[15]Hung, R. J., Lee, C. C., and Leslie, F. W., "Effect of the Baffle on the Spacecraft Fluid Propellant Viscous Stress and Moment Fluctuations," *Transactions of the Japan Society for Aeronautical and Space Sciences*, Vol. 35, No. 2, 1993, pp. 187–207.

[16]Hung, R. J., and Lee, C. C., "Effect of a Baffle on Slosh Waves Excited by Gravity Gradient Acceleration in Microgravity," *Journal of Spacecraft and Rockets*, Vol. 31, No. 6, 1994, pp. 1107–1114.

[17]Greenwood, D. T., *Principles of Dynamics*, Prentice–Hall, Englewood Cliffs, NJ, 1965, p. 518.

[18]Van sciver, S. W., *Helium Cryogenics*, Plenum, New York, 1986, p. 429.

[19]Wilks, J., and Betts, D. S., *An Introduction to Liquid Helium*, Clarendon, Oxford, England, UK, 1987, p. 187.

T. C. Lin
Associate Editor